Sensors & Actuators: B. Chemical 371 (2022) 132527

Contents lists available at ScienceDirect

Sensors and Actuators: B. Chemical

journal homepage: www.elsevier.com/locate/snb

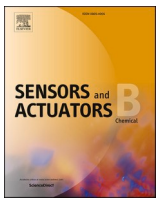

# An ascorbic acid-responsive chemo-chromic SERS sensing chip for synergistic dual-modal on-site analysis of alkaline phosphatase

Jingxing Guo [a,b,1], Yueqin Liu [a,1], Longjiang Zhang [a,b], Jing Pan [a], Yingfei Wang [b], Yiqing Wang [c], Huiming Cai [d], Huangxian Ju [b,*], Guangming Lu [a,b,**]

[a] Department of Medical Imaging, Jinling Hospital, School of Medicine, Nanjing University, Nanjing 210002, PR China
[b] State Key Laboratory of Analytical Chemistry for Life Science, School of Chemistry and Chemical Engineering, Nanjing University, Nanjing 210023, PR China
[c] Biomedical Engineering Department, Nanjing University, Nanjing 210023, PR China
[d] Nanjing Nuoyuan Medical Device Ltd., Nanjing 210014, PR China

ARTICLE INFO

*Keywords:*
Surface-enhanced Raman scattering (SERS)
SERS sensing
Chip
Colorimetry
Core-shell nanoparticles
On-site analysis

ABSTRACT

This work designs an ascorbic acid (AA)-responsive chemo-chromic SERS sensing chip (C-SERS chip) for synergistic dual-modal on-site analysis. This chip can be easily prepared by immobilizing a new kind of core-shell nanoparticles named AuNSs-MBN@Ag@PB on flat filter membrane via vacuum filtration. The reduction of Prussian blue (PB) shell by AA can rapidly change the chip color and enhance SERS signal of 4-mercaptobenzonitrile (MBN), which leads to a synergistic dual-modal sensing strategy for rapid colorimetric screening and SERS quantification of AA-related analytes. Under optimal parameters, the C-SERS chip shows rapid colorimetric response and linear SERS response to AA concentration ranging from 0.5 to 100 μM. The limit of detection for AA is 0.24 μM. The good reproducibility, stability and robustness of the chip and its selectivity to AA demonstrate its practical application in food and biomedical analysis. Using alkaline phosphatase (ALP) as a model analyte, the proposed method with the help of 2-phosphate-*L*-ascorbic acid shows linear SERS response in the range of 0.5–100 U/L ALP. The excellent specificity, high accuracy, satisfactory recovery and convenient operation indicate the potential of the miniaturizable C-SERS chip in high-throughput on-site colorimetric screening and quantitative analysis by combining with a portable Raman spectrometer.

## 1. Introduction

On-site analysis aiming at real time readout, field deployment and easy usage has attracted a lot of attention, especially facing the threaten from COVID-19 [1], and been applied in numerous areas [2]. A qualified analytical strategy for on-site testing needs to be rapid, simple and portable, preferably cost-effective and nondestructive without pretreatment. To meet these requirements, many techniques including colorimetry [3], fluorescence [4], near infrared (NIR) spectroscopy [5], electrochemistry [6] and surface-enhanced Raman scattering (SERS) [7] have been employed in the design of testing schemes. Colorimetry offers rapid and easy-to-read results in low-cost manner but relatively poor sensitivity and quantification performance originated from ambient light interference and inhomogeneous color appearance in the assay regions [8]. SERS represents outstanding sensitivity and selectivity, but it suffers from relatively expensive instruments, long acquisition time and complicated signals for reading [9]. Moreover, most of existing works only use SERS to validate the outcome from other methods and do not let each modality perform its own duty for complementary advantages [10–14]. Thus, the multimodal strategy that integrates these technologies for different purposes of analysis, such as rapid screening and accurate quantification with reduced workload and cost, is an urgent need in on-site analysis [15].

Ascorbic acid (AA), as a well-known vitamin, plays an important role in many biological processes [16]. It can act as strong reducing agent, coenzyme and essential nutritional factor production of certain neurotransmitters [17], and has become a common additive in food, medicine, cosmetics and many other fields [18,19]. Moreover, it can be employed as a reductive component in sensor designs, which are able to extend to monitor other disease biomarkers like alkaline phosphatase (ALP)

* Corresponding author.
** Corresponding author at: Department of Medical Imaging, Jinling Hospital, School of Medicine, Nanjing University, Nanjing 210002, PR China.
*E-mail addresses:* hxju@nju.edu.cn (H. Ju), cjr.luguangming@vip.163.com (G. Lu).
[1] These authors contributed equally to this work

https://doi.org/10.1016/j.snb.2022.132527
Received 9 June 2022; Received in revised form 15 August 2022; Accepted 16 August 2022
Available online 18 August 2022

[20–22], acid phosphatase (ACP) [23] and ascorbic acid oxidase (AAOx) [24]. Therefore, developing fast and sensitive detection methods for AA is of great significance. This work designs an AA-responsive chemo--chromic SERS sensing chip (C-SERS chip) by immobilizing a new kind of core-shell nanoparticles named AuNSs-MBN@Ag@PB (Scheme 1a) on a filter membrane for synergistic dual-modal on-site analysis.

In the core-shell AuNSs-MBN@Ag@PB, 4-mercaptobenzonitrile (MBN) is assembled on gold nanostars (AuNSs) to offer distinct Raman peak of nitrile group (-C≡N), and the presence of Ag nanoparticles not only enhances the SERS signal of MBN due to the Au/Ag hot spots, but also isolates SERS reporter from external interference. Furthermore, the layer-by-layer assembly of nanoparticles can address the limitations resulting from aggregation or deaggregation to SERS sensing [7,25,26]. Prussian blue (PB) as colorimetric reporter is used as the response interface. The AuNSs-MBN@Ag@PB can be densely immobilized on aluminum oxide (AAO) filter membrane to obtain a C-SERS chip. In the presence of AA, the color of C-SERS chip can rapidly change from dark blue to light cyan due to the reduction of PB to colorless Prussian white (PW) [27]. Considering the strong absorption of PB from 650 to 800 nm and its ability to convert light into other forms like thermal energy [28, 29], the outer PB nanoshell of AuNSs-MBN@Ag@PB consumes 785-nm laser and weakens the SERS excitation effect to inner reporter MBN. Thus, the PB-to-PW conversion can also boost the SERS signal intensity of MBN via significantly reducing the absorption of PB [27], leading to the synergistic dual-modal sensing strategy (Scheme 1b). Moreover, the universal AA-responsive chip can be extended to measure other AA-related analytes, such as reactants and corresponding catalysts. Using ALP, the hydrolase of 2-phosphate-*L*-ascorbic acid (AAP), as a model analyte, the analytical results of practical serum samples demonstrate the application of the C-SERS chip with good reproducibility, stability and robustness, and excellent selectivity to targets. The whole analysis process can be completed with a portable Raman spectrometer within 6 min for AA in beverages and 40 min for ALP in serum samples. Thus, this work provides a miniaturizable C-SERS chip for high-throughput on-site colorimetric screening and quantitative analysis in food and clinical diagnosis fields.

## 2. Experimental section

### 2.1. Fabrication of C-SERS chip

The detailed information of AuNSs-MBN@Ag@PB synthesis and characterization are described in the Supplementary materials. Similar to the previous work [26], the C-SERS Chip was prepared by uniformly dropping 100 μL AuNSs-MBN@Ag@PB in ethanol with certain concentrations on AAO filter membrane (pore diameter: 20 nm), which was previously rinsed with ethanol, dried in air and put into a sand cored funnel (G2 porosity). The solvent was pumped out by vacuum suction for 20 s to form a layer of AuNSs-MBN@Ag@PB. After the membrane was washed with ethanol and dried in air, the C-SERS chip was obtained.

### 2.2. SERS characterization of C-SERS chip

The SERS data were collected and analyzed by a Renishaw inVia confocal Raman microscope with accumulation of 1. The SERS signals of AuNSs-MBN, AuNSs-MBN@Ag and AuNSs-MBN@Ag@PB were recorded at random spots on liquid sample under 785 nm at a laser power of 50 mW and exposure time of 10 s. The time series SERS signals for evaluating the stability of AuNSs-MBN@Ag@PB against laser irradiation were collected with an interval of 10 s at one spot on liquid sample under 785 nm laser irradiation for 600 s at a laser power of 500 mW and exposure time of 1 s. The SERS imaging data for evaluating the signal uniformity and reproducibility of C-SERS chip were collected at random areas of 100 μm × 100 μm on chip surface from 2125 to 2200 $cm^{-1}$ using a signal-to-baseline map review mode with exposure time of 1 s. The relative standard deviation (RSD) and average signal intensity were calculated from 441 collection points in each imaging graph.

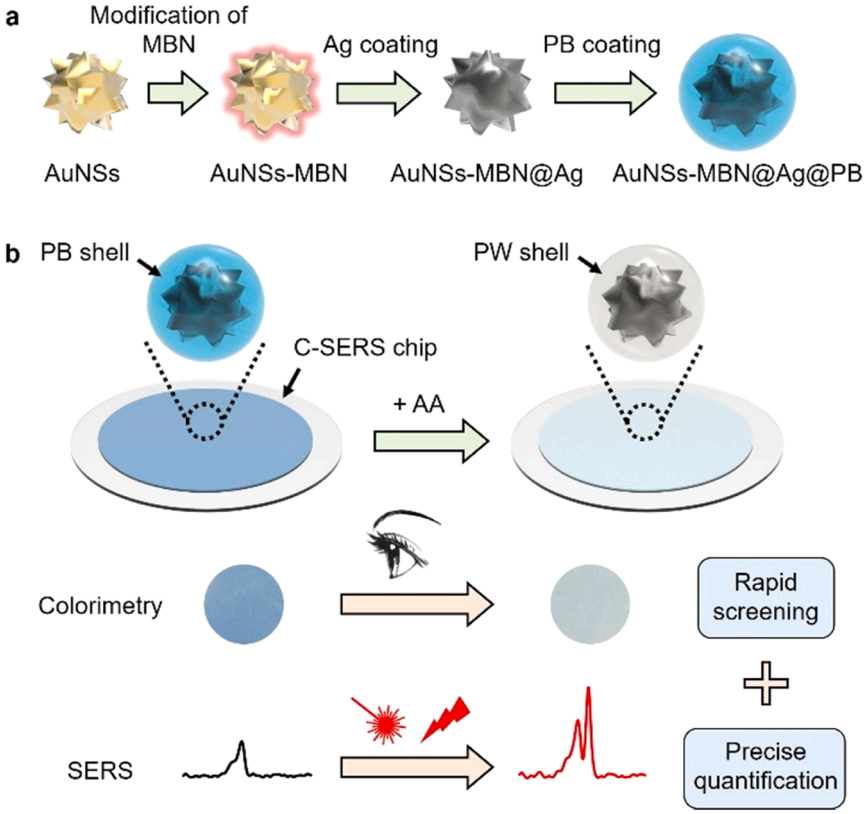


**Scheme 1.** Schematic illustration of (a) preparation of AuNSs-MBN@Ag@PB and (b) synergistic colorimetry and SERS dual-modal on-site analysis.

### 2.3. Colorimetric and SERS sensing of AA

The colorimetric and SERS responses of AuNSs-MBN@Ag@PB to AA were examined by mixing 100 μM of AA with AuNSs-MBN@Ag@PB in PBS (pH 7.4) to react for 5 min under room temperature. The nanoparticles were then washed three times by centrifugation (6000 rpm, 10 min) and redispersed in water for subsequent characterizations.

For evaluating the sensing performance of the C-SERS chip, it was directly immersed in PBS (pH 7.4) containing certain concentration of

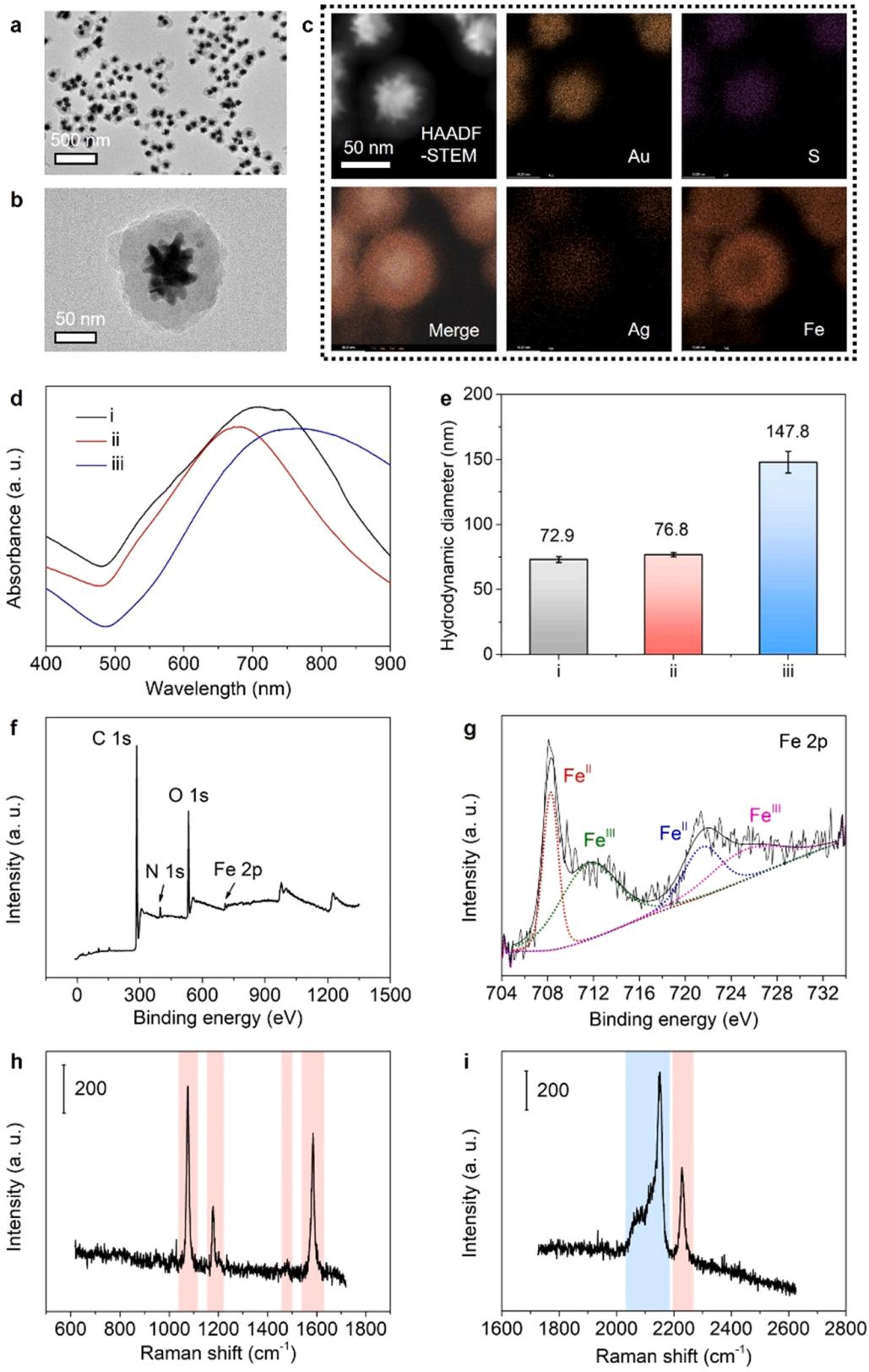


**Fig. 1.** Characterization of AuNSs-MBN@Ag@PB. TEM images of AuNSs-MBN@Ag@PB in (a) low and (b) high magnification. (c) HAADF-STEM image of AuNSs-MBN@Ag@PB and corresponding EDX elemental mapping of Au, S, Ag and Fe, and the merged image. (d) UV–vis spectra of AuNSs-MBN (i), AuNSs-MBN@Ag (ii) and AuNSs-MBN@Ag@PB (iii). (e) Hydrodynamic diameters of i, ii and iii. The error bars indicate means ± s.d. ($n = 3$). (f) XPS survey spectrum, (g) Fe 2p XPS spectrum, and (h, i) typical SERS spectra of AuNSs-MBN@Ag@PB. The red and blue regions indicate the characteristic peaks of MBN and PB, respectively. Excitation laser: 785 nm; laser power: 50 mW; exposure time: 10 s; accumulation: 1.

AA for 5 min under room temperature. The chip was then washed with water and ethanol successively for subsequent dual-model signal readout. The same procedures were used for evaluating the selectivity of C-SERS chip. To detect the AA content in beverages, the samples were diluted 20 times with PBS (pH 7.4) to perform the same procedures. The optical images of chips were taken with an iPhone 12 Pro Max smartphone without using flash light. The focusing point was manually set at the chip center, and the shooting parameters like the contrast and brightness values were automatically set by the phone. For reliable colorimetric assays, the shooting position and ambient light were consistent on each photograph and the gray values were analyzed with Image J software. The SERS data were collected at random spots on chip surface by a Portman785 Portable Raman spectrometer under 785 nm at a laser power of 50 mW and an exposure time of 1 s with 5 accumulations.

### 2.4. Colorimetric and SERS sensing of ALP

The sample containing ALP was firstly mixed with 1 mM AAP in tris-HCl buffer (pH 8.0) to react for 30 min under 37 ℃. Afterward, the chip was directly immersed in the mixture for 5 min, and washed with ethanol and water successively for subsequent dual-model signal readout. For the detection of ALP in human serums, the serum samples were diluted 2 times with tris-HCl buffer (pH 8.0) to perform the same procedures. The SERS data were collected at random spots on chip surface by a Portman785 Portable Raman spectrometer under 785 nm at a laser power of 50 mW and an exposure time of 1 s with 5 accumulations.

## 3. Results and discussion

### 3.1. Preparation and characterization of AuNSs-MBN@Ag@PB

The presence of nitrile group (-C≡N) in MBN molecule offers distinct Raman peak in biosilent region, which is very suitable to SERS reporter for reducing the interference from sample matrix [30]. Due to the outstanding SERS performance that originates from the sharp tips [31], AuNSs were chosen as SERS substrate to assemble MBN via Au-S bonding. Under optimal MBN concentration for modification and thickness of Ag shell (Figs. S1-S3), the obtained AuNSs-MBN@Ag showed the maximal peak intensity at 2228 $cm^{-1}$ (Fig. S4). AuNSs-MBN@Ag@PB could be easily prepared by adding precursors of $FeCl_3$/$K_4[Fe(CN)_6]$ into AuNSs-MBN@Ag for forming PB shell as colorimetric reporter. It owned well-defined core-shell structure and uniform size about 120 nm in diameter (Fig. 1a and b). The typical core-shell morphology with Au and S atoms in the core, and Ag and Fe atoms homogeneously covering the core in sequence matched well with its nanostructure (Fig. 1c). The ICP-AES analysis also confirmed the presence of Au, S, Ag and Fe elements in the nanoparticles (Table S1).

AuNSs-MBN showed an absorbance peak at 709 nm, which obviously blue-shifted to 679 nm after Ag coating (Fig. 1d). Interestingly, the absorbance peak of the nanoparticles was broadened and red-shifted to 763 nm after PB coating, which could be attributed to the mixed-valence charge-transfer absorbance around 700 nm of the polymeric [$Fe^{II}$-C≡N-$Fe^{III}$] in PB [32]. The successive formation of Ag and PB shells increased the hydrodynamic diameter from 72.9 nm of AuNSs-MBN, 76.8 nm of AuNSs-MBN@Ag to 147.8 nm of AuNSs-MBN@Ag@PB (Fig. 1e).

The X-ray photoelectron spectrum (XPS) of AuNSs-MBN@Ag@PB showed the presence of Fe element (Fig. 1f) with two states, $Fe^{II}$ at ca 0.708.3 eV and ca 0.721.5 eV, and $Fe^{III}$ at ca 0.711.6 eV and ca 0.725.2 eV (Fig. 1g), indicating the existence of PB shell [33,34]. The AuNSs-MBN@Ag@PB represented the strong SERS peaks of MBN at 1076 ($\nu$(C-S) of aromatic ring), 1178 ($\delta$(C-H) of aromatic ring), 1480 and 1586 ($\nu$(C-C) of aromatic ring), and 2228 $cm^{-1}$ ($\nu$(C≡N)) [35], as well as SERS peaks of PB at 2150 $cm^{-1}$ ($\nu$($Fe^{II}$-C≡N-$Fe^{III}$)) (Fig. 1h and 1i) [36]. These results verified the successful preparation of AuNSs-MBN@Ag@PB. It is worth noting that the outer shell could isolate the inner SERS reporter from external chemical environment and maintain signal reproducibility and stability against interferences, such as photothermal damage during laser irradiation. Thus, the MBN signal fluctuation of AuNSs-MBN@Ag@PB was very little, which showed an RSD of only 6.73% under continuous 785 nm laser irradiation with 500 mW for 600 s (Fig. S5). This impressive signal stability guaranteed the high-quality SERS measurements for target quantification.

### 3.2. Feasibility of dual-modal responses of AuNSs-MBN@Ag@PB to AA

The feasibility of AuNSs-MBN@Ag@PB responsive to AA was evaluated by mixing 100 μM of AA and AuNSs-MBN@Ag@PB. After mixing two solutions for only 5 min, the dark blue solution faded and the broad absorbance around 763 nm reduced to 43.54% (Fig. 2a and b), implying the conversion of PB to colorless PW due to the reduction of PB by AA [37], providing a colorimetric method for AA screening. Meanwhile, a shoulder SERS peak assigned to $\nu$($Fe^{II}$-C≡N-$Fe^{II}$) appeared at 2120 $cm^{-1}$ and a weak peak related to PW also occurred at 2095 $cm^{-1}$ after adding 100 μM AA [38,39], which further confirmed the AA-induced PB-to-PW conversion (Fig. 2c). After this conversion, the core-shell nanostructure of AuNSs-MBN@Ag@PB could be maintained (Fig. S6). More importantly, the conversion could sensitively boost the SERS signal intensity of inner reporter MBN at different peak positions including 2228 $cm^{-1}$ (Fig. 2d). The rapid and significant response to AA observed by naked eyes and portable Raman spectrometer provides a possibility to using AuNSs-MBN@Ag@PB for dual-modal on-site analysis.

### 3.3. Characterization of C-SERS chip

A dense nanoparticle layer on AAO filter membrane could be rapidly obtained via vacuum filtration [26]. Thus, it was used to fabricate C-SERS chip for dual-modal analysis. Considering the effect of color shade on colorimetric results, the amount of AuNSs-MBN@Ag@PB for C-SERS chip fabrication was firstly optimized to be 20 fmol, at which the obtained chip showed uniform dark blue of PB shell (Fig. 3a), and the maximal color difference upon reaction with 100 μM of AA (Fig. S7). The chip also owned distinct SERS peaks of MBN at 1072, 1182, 1489, 1582 and 2220 $cm^{-1}$, as well as PB at 2138 $cm^{-1}$ (Fig. 3b). The little difference of peak positions to colloid AuNSs-MBN@Ag@PB may due to the dense aggregation state on AAO membrane.

As a practical sensor for on-site analysis, the signal uniformity, reproducibility, stability and robustness of C-SERS chip was further evaluated. The chips fabricated from three batches displayed similar appearance and the average SERS signal intensity of PB at 2138 $cm^{-1}$. Each one of the chips also presented satisfied signal uniformity with RSD of 13.1 %, 13.7 % and 13.0 % in 100 μm × 100 μm area, respectively (Fig. S8). Furthermore, no obvious SERS signal change of the chip was observed after one week of storage under room temperature or successively rinsing with water and ethanol for 30 s, indicating potential durability for deploying on field (Fig. S9).

### 3.4. Colorimetric and SERS sensing of AA with C-SERS chip

To assess the performance of C-SERS chip for AA detection, it was directly immersed in buffer solution spiked with different concentrations of AA to react for only 5 min. With the increasing AA concentration from 0 to 200 μM, the color of C-SERS chip gradually faded and changed from dark blue to light cyan (Fig. 3c), which could conveniently be used to notify the presence of AA and evaluate the concentration variation of AA by naked eyes or colorimetric measurements of average gray values, which showed a linear correlation ranging from 5.0 to 100 μM with $R^2$ of 0.9705 (Fig. S10). The chip color hardly changed when AA concentration was larger than 200 μM.

The SERS peak intensity at 2220 $cm^{-1}$ of MBN increased with the increasing AA concentration and tended to saturation until 200 μM of

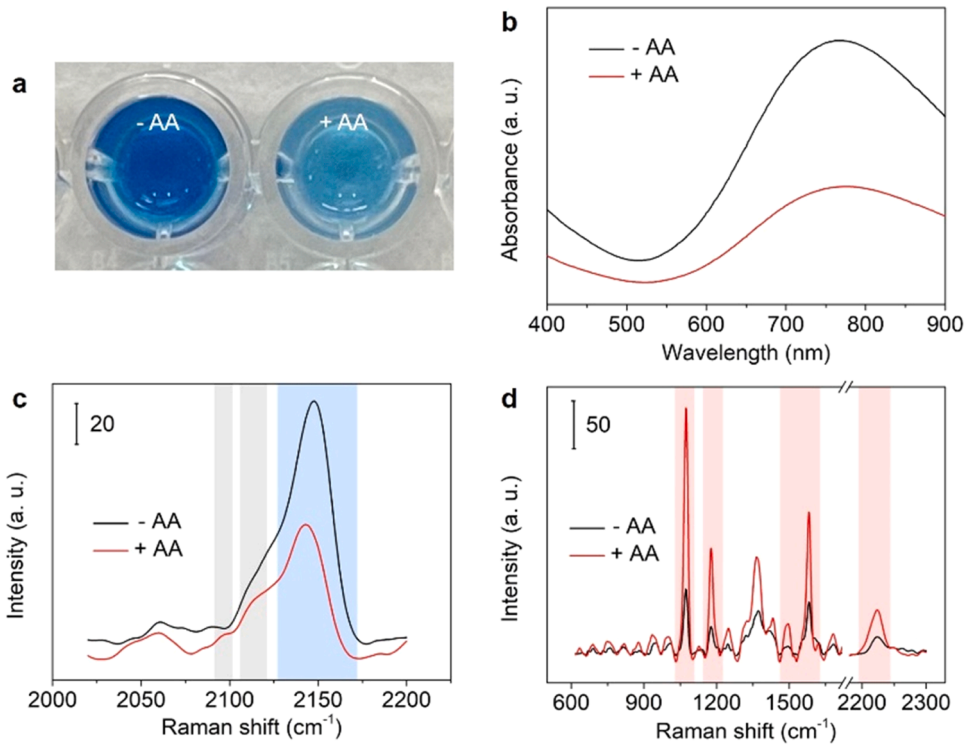


**Fig. 2.** Feasibility of AuNSs-MBN@Ag@PB response to AA. (a) Optical image, (b) UV–vis spectra and (c, d) typical SERS spectra of AuNSs-MBN@Ag@PB in absence or presence of 100 μM AA. The red, blue and gray regions indicate the characteristic peaks of MBN, PB and PW, respectively. Excitation laser: 785 nm; laser power: 50 mW; exposure time: 10 s; accumulation: 1.

AA, leading to a good linear range from 0.5 to 100 μM with $R^2$ of 0.9933 (Fig. 3d and e). As expected, all SERS peaks of MBN were gradually enhanced with the increasing AA concentration, verifying the boosted SERS signal intensity since PB-to-PW conversion (Fig. S11). The limit of detection (LOD) for AA was calculated to be 0.24 μM, which was comparable or lower than many recent strategies based on electrochemistry [40], fluorescence [18], photothermal [41] or even SERS [19]. This superior performance originated from the interference-free signals of MBN embedded into hot spots of nanoparticles. It is worth noting that the SERS represented much better signal reproducibility and sensitivity than colorimetric results, which was more qualified for precise quantification.

Various potential coexisting interferents, including metal ions such as $Na^+$, $K^+$ and $Ca^{2+}$, carbohydrates such as glucose and fructose, amino acids such as *L*-serine (*L*-Ser), *L*-glutamic acid (*L*-Glu) and *L*-histidine (*L*-His), and other reductants such as glutathione, uric acid, dopamine and salicylic acid, were employed to test the specificity of C-SERS chip. As shown in Fig. 3f, the significant changes of color and SERS peak intensity only appeared for AA, indicating impressive selectivity to the target.

The practical application of C-SERS chip was demonstrated by detecting AA contents in beverages without pretreatment. As illustrated in Table 1, the presence and content difference of AA could be easily screened by chip colors, which showcased the similar cyan for Minute Maid@ "Qing Qing De Ning" and "Guo Li Cheng", whereas lighter cyan for Nongfu Spring@ "C100″. SERS was responsible for the further precise quantification of AA, and the test results were in good agreement with the nutrition facts labels. After spiking certain concentrations of AA in these samples, satisfactory recoveries of 96.9–104.6 % with RSD less than 4.94 % were achieved. The colorimetric screening within 5 min combined with sensitive and portable SERS quantification offered a comprehensive testing scheme for AA on-site analysis.

### 3.5. Colorimetric and SERS sensing of ALP with C-SERS ship

Considering the sensitive and selective response to AA, C-SERS chip can also extend to analyze other targets like ALP, which is capable to specifically hydrolyze AAP into AA. The feasibility was verified via directly immersing the chip into the buffer solution containing ALP and/or AAP, which was incubated under 37 ℃ for 30 min beforehand. After 5-min immersion, the chip color faded and SERS peak intensity of MBN increased only when ALP and AAP co-existed (Fig. 4a-c). To obtain the best sensing performance of ALP, the concentration of AAP used in measurements was optimized to be 1 mM (Fig. S12), at which the color of C-SERS chip gradually changed from dark blue to almost gray, and the SERS peak intensity of MBN at 2220 $cm^{-1}$ increased with the increasing ALP concentration from 0 to 100 U/L (Fig. 4d-f). The plot of SERS peak intensity vs ALP concentration showed a good linearity in the range of 0.5–100 U/L with $R^2$ of 0.9895. The LOD was calculated to be 0.35 U/L, which was totally enough to analyze real human samples (38–126 U/L) and comparable to many reported works [20,21,42]. The C-SERS chip also owned excellent selectivity for dual-modal detection of ALP when it faced potential interferents such as bovine serum albumin (BSA), glucose oxidase (GOx), horseradish peroxidase (HRP) and lysozyme (Fig. 4g). Besides, no obvious detachment of AuNSs-MBN@Ag@PB from chip surface was observed after the chip was immersed in AA or ALP solutions, guaranteeing the reliability for testing samples (Fig. S13).

The potential of the proposed method in on-site analysis of ALP level in real samples was demonstrated. As expected, the chip could not only verify the presence of ALP but also distinguish the normal from abnormal samples by naked eyes, which was very meaningful for rapid screening (Table 2). The precise quantification of ALP activity was achieved with SERS measurements and the test results were in good agreement with the traditional photometry carried out by clinicians. The results showed satisfactory recoveries of about 97 % with RSDs less than 5.53 %. It is worth stressing that the whole analytical procedure could be completed within 40 min, the equipment used for fabrication and

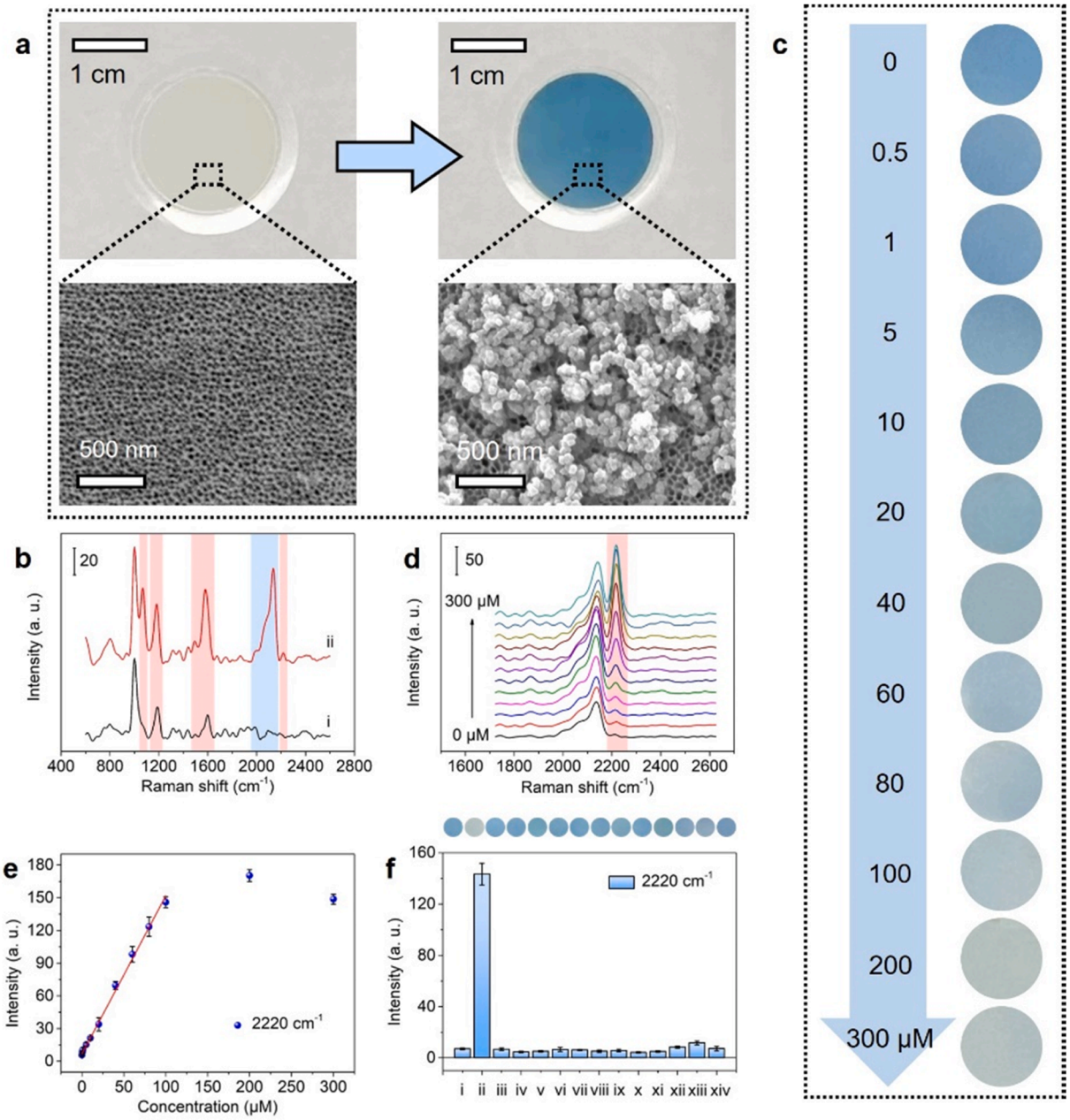


**Fig. 3.** Dual-modal sensing of AA with C-SERS chip. (a) Optical and SEM images of AAO filter membrane before and after AuNSs-MBN@Ag@PB immobilization. (b) Raman spectrum of AAO filter membrane (i) and SERS spectrum of C-SERS chip (ii). (c) Optical images and (d) SERS spectra of C-SERS chip responding to AA from 0 to 300 μM. (e) Linear calibration plot of SERS peak intensity at 2220 $cm^{-1}$ vs AA concentration. (f) Optical images and SERS peak intensity at 2220 $cm^{-1}$ responding to 1 × PBS as blank, 100 μM of AA, and 1 mM of $Na^+$, $K^+$, $Ca^{2+}$, glucose, fructose, *L*-Ser, *L*-Glu, *L*-His, glutathione, uric acid, dopamine and salicylic acid (i-xiv). The red and blue regions indicate the characteristic peaks of MBN and PB, respectively. The error bars indicate means ± s.d. ($n = 5$). Excitation laser: 785 nm; laser power: 50 mW; exposure time: 1 s; accumulation: 5.

measurements was simple, and the chip was miniaturizable, which manifested the strong ability for point-of-care testing (Fig. S14).

## 4. Conclusion

This work designs a synergistic dual-modal C-SERS chip by conveniently immobilizing novel core-shell nanoparticles named AuNSs-MBN@Ag@PB on AAO filter membrane for on-site analysis. The AuNSs-MBN@Ag@PB can be easily synthesized by assembling MBN on AuNSs via Au-S bonding, and successively depositing Ag and PB shell on AuNSs-MBN. Due to the PB-to-PW conversion resulted from PB reduction by AA, the color of this chip can rapidly change and the SERS signal of inner MBN simultaneously enhances, which leads to a dual-modal sensing strategy integrating rapid colorimetric screening and SERS quantification for AA detection. This strategy possesses good extendibility for AA-related analytes, such as reactants and corresponding catalysts, which has been demonstrated with a proposed detection method for ALP. The C-SERS chip represents good reproducibility, stability, robustness, and excellent selectivity toward AA. The analytical results of the real samples like beverages and human serums demonstrate the promising potential of the proposed chip and dual-modal strategy in on-site analysis of food and clinical diagnosis fields.

## CRediT authorship contribution statement

**Jingxing Guo**: Conceptualization, Methodology, Investigation,

**Table 1**
Detection of AA content in beverages with C-SERS chip.

| Beverage sample | Founded (mg/100 mL) | Spiked (mg/100 mL) | Measured value (mg/100 mL) | Recovery (%) | RSD ($n = 5$, %) | Optical image |
|---|---|---|---|---|---|---|
| Blank | 0 | 0 | – | – | – | |
| Minute Maid@ "Qing Qing De Ning" | 7.5 | 0 | 7.9 | – | 3.93 | |
| | | 7.0 | 14.6 | 101.2 | 4.54 | – |
| | | 14.0 | 21.8 | 102.5 | 4.83 | – |
| | | 21.0 | 28.1 | 97.9 | 2.42 | – |
| Minute Maid@ "Guo Li Cheng" | 7.5 | 0 | 7.3 | – | 2.49 | |
| | | 7.0 | 14.4 | 98.3 | 4.94 | – |
| | | 14.0 | 21.9 | 103.5 | 2.72 | – |
| | | 21.0 | 28.0 | 97.7 | 4.67 | – |
| Nongfu Spring@ "C100" | 22.5 | 0 | 23.0 | – | 4.49 | |
| | | 7.0 | 29.8 | 104.6 | 2.40 | – |
| | | 14.0 | 36.1 | 96.9 | 2.96 | – |
| | | 21.0 | 43.6 | 100.8 | 3.52 | – |

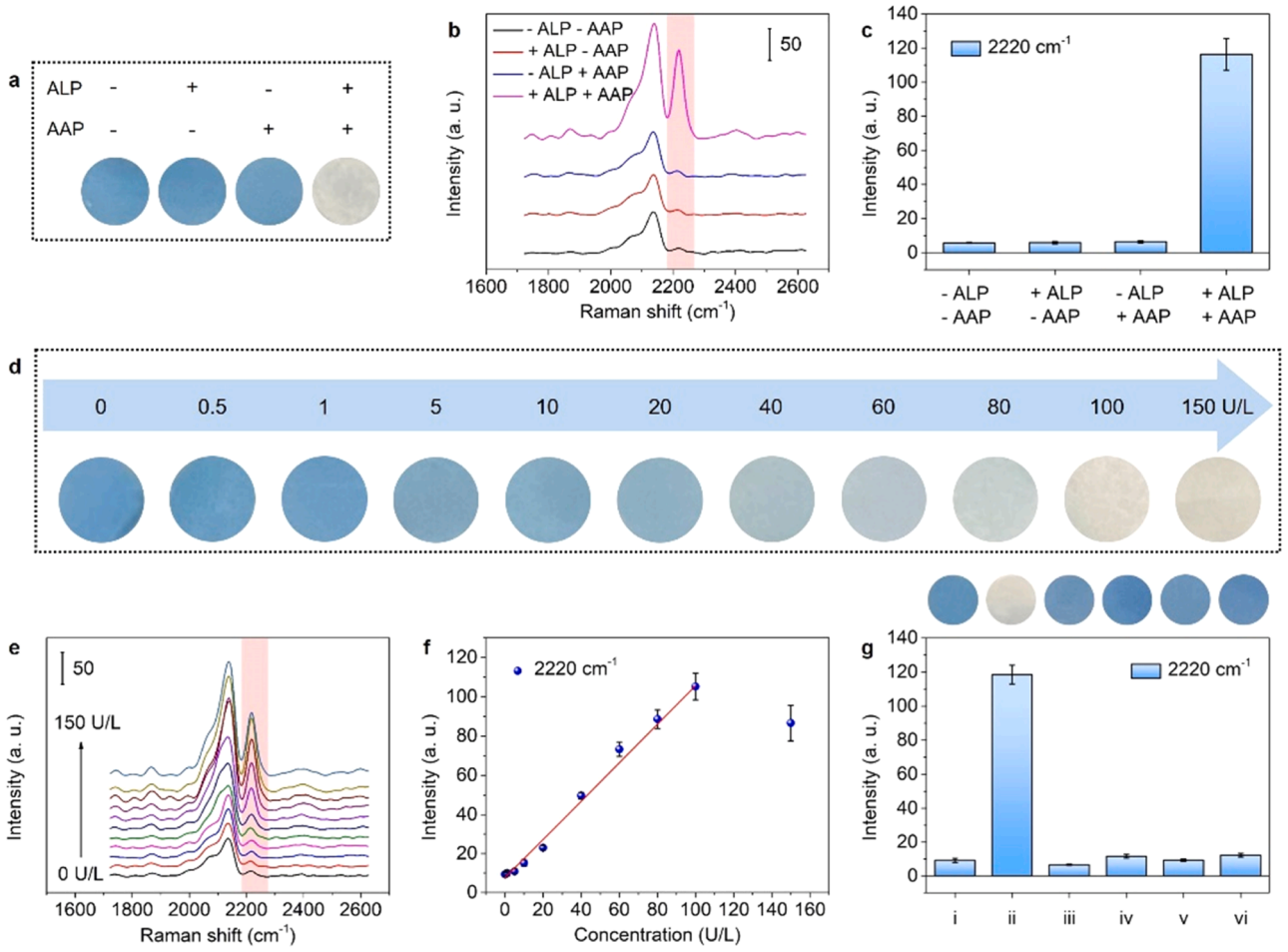


**Fig. 4.** Dual-modal sensing of ALP with C-SERS chip. (a) Optical images, (b) SERS spectra, and (c) SERS peak intensity at 2220 $cm^{-1}$ responding to blank, 100 U/L ALP, 1 mM AAP or mixture of 100 U/L ALP and 1 mM AAP. (d) Optical images and (e) SERS spectra of C-SERS chip responding to ALP from 0 to 150 U/L in presence of 1 mM AAP. (f) Plot of SERS peak intensity at 2220 $cm^{-1}$ vs ALP concentration. (g) Optical images and SERS peak intensity at 2220 $cm^{-1}$ responding to 1 × PBS as blank, 100 U/L ALP, 1 mg/mL BSA, 1000 U/L GOx, 1000 U/L HRP and 1000 U/L lysozyme (i-vi). The red region indicates the characteristic peak of MBN. The error bars indicate means ± s.d. ($n = 5$). Excitation laser: 785 nm; laser power: 50 mW; exposure time: 1 s; accumulation: 5.

**Table 2**
Evaluation of ALP levels in human serum samples with C-SERS chip.

| Serum samples | Founded (U/L) | Spiked (U/L) | Measured value (U/L) | Recovery (%) | RSD ($n = 3$, %) | Optical image |
|---|---|---|---|---|---|---|
| Blank | 0 | 0 | – | – | – |  |
| 1 (Male) | 107 | 0 | 110 | – | 5.53 |  |
| 2 (Male) | 107 | 75 | 179 | 96.2 | 4.09 |  |
| 3 (Female) | 65 | 0 | 68 | – | 5.01 |  |
| 4 (Female) | 65 | 100 | 163 | 96.9 | 4.48 |  |

Writing – original draft and Funding acquisition. **Yueqin Liu**: Methodology, Investigation and Writing – original draft. **Longjiang Zhang**: Validation and Resources. **Jing Pan**: Investigation. **Yingfei Wang**: Investigation. **Yiqing Wang**: Resources. **Huiming Cai**: Resources. **Huangxian Ju**: Conceptualization, Supervision and Writing – review & editing. **Guangming Lu**: Conceptualization, Supervision, Writing – review & editing and Funding acquisition.

## Declaration of Competing Interest

The authors declare that they have no known competing financial interests or personal relationships influencing the work reported in this paper.

## Data availability

No data was used for the research described in the article.

## Acknowledgments

This work was financially supported by National Natural Science Foundation of China (82127806), China Postdoctoral Science Foundation (2020M683717), Postdoctoral Science Foundation of Jiangsu Province (2020Z142) and State Key Laboratory of Analytical Chemistry for Life Science (SKLACLS2104).

## Appendix A. Supporting information

Supplementary data associated with this article can be found in the online version at doi:10.1016/j.snb.2022.132527.

## References

[1] S. Shrivastava, T.Q. Trung, N.-E. Lee, Recent progress, challenges, and prospects of fully integrated mobile and wearable point-of-care testing systems for self-testing, Chem. Soc. Rev. 49 (2020) 1812–1866.
[2] J.X. Guo, Y. Liu, H.X. Ju, G.M. Lu, From lab to field: Surface-enhanced Raman scattering-based sensing strategies for on-site analysis, Trends Anal. Chem. 146 (2022), 116488.
[3] Z. Li, J.R. Askim, K.S. Suslick, The optoelectronic nose: colorimetric and fluorometric sensor arrays, Chem. Rev. 119 (2019) 231–292.
[4] M.Z. Yang, Y. Liu, X.Y. Jiang, Barcoded point-of-care bioassays, Chem. Soc. Rev. 48 (2019) 850–884.
[5] S. Pahlow, K. Weber, J. Popp, B.R. Wood, K. Kochan, A. Rüther, D. Perez-Guaita, P. Heraud, N. Stone, A. Dudgeon, B. Gardner, R. Reddy, D. Mayerich, R. Bhargava, Application of vibrational spectroscopy and imaging to point-of-care medicine: a review, Appl. Spectrosc. 72 (2018) 52–84.
[6] N. Wongkaew, M. Simsek, C. Griesche, A.J. Baeumner, Functional nanomaterials and nanostructures enhancing electrochemical biosensors and lab-on-a-chip performances: recent progress, applications, and future perspective, Chem. Rev. 119 (2019) 120–194.
[7] J.X. Guo, Y. Liu, Y.L. Chen, J.Q. Li, H.X. Ju, A multifunctional SERS sticky note for real-time quorum sensing tracing and inactivation of bacterial biofilms, Chem. Sci. 9 (2018) 5906–5911.
[8] K. Yamada, T.G. Henares, K. Suzuki, D. Citterio, Paper-based inkjet-printed microfluidic analytical devices, Angew. Chem. Int. Ed. 54 (2015) 5294–5310.
[9] C. Zong, M.X. Xu, L.-J. Xu, T. Wei, X. Ma, X.-S. Zheng, R. Hu, B. Ren, Surface-enhanced Raman spectroscopy for bioanalysis: reliability and challenges, Chem. Rev. 118 (2018) 4946–4980.
[10] J.H. Liu, J.H. Chen, D. Wu, M.Q. Huang, J. Chen, R.Y. Pan, Y.N. Wu, G.L. Li, CRISPR-/Cas12a-mediated liposome-amplified strategy for the surface-enhanced Raman scattering and naked-eye detection of nucleic acid and application to food authenticity screening, Anal. Chem. 93 (2021) 10167–10174.
[11] L.H. Su, H.L. Hu, Y.L. Tian, C.H. Jia, L.L. Wang, H. Zhang, J.L. Wang, D.H. Zhang, Highly sensitive colorimetric/surface-enhanced Raman spectroscopy immunoassay relying on a metallic core-shell Au/Au nanostar with clenbuterol as a target analyte, Anal. Chem. 93 (2021) 8362–8369.
[12] B.W. Zhao, S.L. Feng, Y.X. Hua, S. Wang, X.N. Lu, Rapid determination of atrazine in apple juice using molecularly imprinted polymers coupled with gold nanoparticles-colorimetric/SERS dual chemosensor, Food Chem. 276 (2019) 366–375.
[13] J.H. Wang, J.M. Wu, Y.P. Zhang, X. Zhou, Z.W. Hu, X.J. Liao, B.B. Sheng, K. S. Yuan, X.Q. Wu, H.H. Cai, H.B. Zhou, P.H. Sun, Colorimetric and SERS dual-mode sensing of mercury (II) based on controllable etching of Au@Ag core/shell nanoparticles, Sens. Actuators B Chem. 330 (2021), 129364.
[14] D.D. Men, G.Q. Liu, C.H. Xing, H.H. Zhang, J.H. Xiang, Y.Q. Sun, L.F. Hang, Dynamically tunable plasmonic band for reversible colorimetric sensors and surface-enhanced Raman scattering effect with good sensitivity and stability, ACS Appl. Mater. Interfaces 12 (2020) 7494–7503.
[15] Y. Zhang, S.J. Zhao, J.K. Zheng, L.L. He, Surface-enhanced Raman spectroscopy (SERS) combined techniques for high-performance detection and characterization, Trends Anal. Chem. 90 (2017) 1–13.
[16] K.-T. Khaw, S. Bingham, A. Welch, R. Luben, N. Wareham, S. Oakes, N. Day, Relation between plasma ascorbic acid and mortality in men and women in EPIC-Norfolk prospective study: a prospective population study, Lancet 357 (2001) 657–663.
[17] J. Scheffler, K. Bork, V. Bezold, P. Rosenstock, V.S. Gnanapragassam, R. Horstkorte, Ascorbic acid leads to glycation and interferes with neurite outgrowth, Exp. Gerontol. 117 (2019) 25–30.
[18] L. Gu, J.R. Zhang, G.X. Yang, Y.Y. Tang, X. Zhang, X.Y. Huang, W.L. Zhai, E. K. Fodjo, C. Kong, Green preparation of carbon quantum dots with wolfberry as on-off-on nanosensors for the detection of $Fe^{3+}$ and *L*-ascorbic acid, Food Chem. 376 (2022), 131898.
[19] W. Wang, Y. Zhang, W. Zhang, Y.B. Liu, P.Y. Ma, X.H. Wang, Y. Sun, D.Q. Song, A novel sensing platform for the determination of alkaline phosphatase based on SERS-fluorescent dual-mode signals, Anal. Chim. Acta 1183 (2021), 338989.
[20] L.P. Zhang, Y. Li, G.E. Mu, L.J. Yang, C.H. Ren, Z.Y. Wang, Q.X. Guo, J.F. Liu, C. H. Yang, Structure of self-assembled peptide determines the activity of aggregation-induced emission luminogen-peptide conjugate for detecting alkaline phosphatase, Anal. Chem. 94 (2022) 2236–2243.
[21] L.P. Gao, Y. Li, Z.-Z. Huang, H.L. Tan, Visual detection of alkaline phosphatase based on ascorbic acid-triggered gel-sol transition of alginate hydrogel, Anal. Chim. Acta 1148 (2021), 238193.
[22] F.N. Lu, M.-J. Wu, C.-J. Yu, X.L. Gao, H. Zhou, Z.Q. Yuan, Colorimetric alkaline phosphatase activity detection by integrating phosphorylation-mediated sulfydryl protection/deprotection and fluorosurfactant stabilized gold nanoparticles, Sens. Actuators B Chem. 325 (2020), 128959.
[23] J. Li, Y.-Y. Wei, Z.-R. Xu, Visual detection of acid phosphatase based on hollow mesoporous manganese dioxide nanospheres, Anal. Chim. Acta 1138 (2020) 1–8.
[24] N. Li, F. Zhang, W.Y. Sun, L.L. Zhang, X.G. Su, Redox reaction-modulated fluorescence biosensor for ascorbic acid oxidase assay by using $MoS_2$ quantum dots as fluorescence probe, Talanta 222 (2021), 121522.

[25] J.X. Guo, Z.H. Zhong, Y.M. Li, Y. Liu, R.Y. Wang, H.X. Ju, "Three-in-one" SERS adhesive tape for rapid sampling, release, and detection of wound infectious pathogens, ACS Appl. Mater. Interfaces 11 (2019) 36399–36408.
[26] J.X. Guo, Y. Liu, Y.J. Yang, Y.M. Li, R.Y. Wang, H.X. Ju, A filter supported surface-enhanced Raman scattering "nose" for point-of-care monitoring of gaseous metabolites of bacteria, Anal. Chem. 92 (2020) 5055–5063.
[27] X.Y. Zhang, H.H. Rao, H.Y. Huang, K.H. Zhang, M.M. Wei, M.Y. Luo, X. Xue, Z. H. Xue, X.Q. Lu, A sensitive photothermometric biosensor based on redox reaction-controlled nanoprobe conversion from Prussian blue to Prussian white, Anal. Bioanal. Chem. 413 (2021) 6627–6637.
[28] Z.Z. Yu, W.B. Hu, H. Zhao, X.F. Miao, Y. Guan, W.Z. Cai, Z.P. Zeng, Q.L. Fan, T.T. Y. Tan, Generating new cross-relaxation pathways by coating Prussian blue on $NaNdF_4$ to fabricate enhanced photothermal agents, Angew. Chem. Int. Ed. 58 (2019) 8536–8540.
[29] X.J. Cai, W. Gao, L.L. Zhang, M. Ma, T.Z. Liu, W.X. Du, Y.Y. Zheng, H.R. Chen, J. L. Shi, Enabling Prussian blue with tunable localized surface plasmon resonances: simultaneously enhanced dual-mode imaging and tumor photothermal therapy, ACS Nano 10 (2016) 11115–11126.
[30] X.-R. Bai, L.-H. Wang, J.-Q. Ren, X.-W. Bai, L.-W. Zeng, A.-G. Shen, J.-M. Hu, Accurate clinical diagnosis of liver cancer based on simultaneous detection of ternary specific antigens by magnetic induced mixing surface-enhanced Raman scattering emissions, Anal. Chem. 91 (2019) 2955–2963.
[31] W.X. Niu, Y.A.A. Chua, W.Q. Zhang, H.J. Huang, X.M. Lu, Highly symmetric gold nanostars: crystallographic control and surface-enhanced Raman scattering property, J. Am. Chem. Soc. 137 (2015) 10460–10463.
[32] J.-D. Qiu, H.-Z. Peng, R.-P. Liang, J. Li, X.-H. Xia, Synthesis, characterization, and immobilization of Prussian blue-modified Au nanoparticles: application to electrocatalytic reduction of $H_2O_2$, Langmuir 23 (2007) 2133–2137.
[33] F.F. Chen, L.L. Teng, C. Lu, C. Zhang, Q.M. Rong, Y. Zhao, Y. Yang, Y.J. Wang, G. S. Song, X.B. Zhang, Activatable magnetic/photoacoustic nanoplatform for redox-unlocked deep-tissue molecular imaging in vivo via Prussian blue nanoprobe, Anal. Chem. 92 (2020) 13452–13461.
[34] W.O. Silva, V.C. Bassetto, D. Baster, M. Mensi, E. Oveisi, H.H. Girault, Oxidative print light synthesis thin film deposition of Prussian blue, ACS Appl. Electron. Mater. 2 (2020) 927–935.
[35] D. Gkogkou, B. Schreiber, T. Shaykhutdinov, H.K. Ly, U. Kuhlmann, U. Gernert, S. Facsko, P. Hildebrandt, N. Esser, K. Hinrichs, I.M. Weidinger, T.W.H. Oates, Polarization- and wavelength-dependent surface-enhanced Raman spectroscopy using optically anisotropic rippled substrates for sensing, ACS Sens. 1 (2016) 318–323.
[36] W. Zhu, M.-Y. Gao, Q. Zhu, B. Chi, L.-W. Zeng, J.-M. Hua, A.-G. Shen, Monodispersed plasmonic Prussian blue nanoparticles for zero-background SERS/MRI-guided phototherapy, Nanoscale 12 (2020) 3292–3301.
[37] H.H. Xing, X.W. Zhang, Q.F. Zhai, J. Li, E. Wang, Bipolar electrode based reversible fluorescence switch using Prussian blue/Au nanoclusters nanocomposite film, Anal. Chem. 89 (2017) 3867–3872.
[38] S. Nappini, A. Matruglio, D. Naumenko, S.D. Zilio, M. Lazzarino, F.M.F. De Groot, C. Kocabas, O. Balci, E. Magnano, Graphene nanoreactors: photoreduction of Prussian blue in aqueous solution, J. Phys. Chem. C 121 (2017) 22225–22233.
[39] R. Mažeikienė, G. Niaura, A. Malinauskas, Electrocatalytic reduction of hydrogen peroxide at Prussian blue modified electrode: an in situ Raman spectroelectrochemical study, J. Electroanal. Chem. 660 (2011) 140–146.
[40] L.H. Li, P. Zhang, Z.Y. Li, D.Y. Li, B. Han, L. Tu, B. Li, Y.G. Wang, L. Ren, P.Y. Yang, S.K. Ke, S.F. Ye, W. Shi, CuS/Prussian blue core-shell nanohybrid as an electrochemical sensor for ascorbic acid detection, Nanotechnology 30 (2019), 325501.
[41] K.X. Wei, H.H. Rao, X. Xue, M.Y. Luo, Z.H. Xue, A facile photothermometric sensor of acid phosphatase based on CoOOH nanozymes-mediated 3,3′,5,5′-tetramethylbenzidine photothermal system, Microchem. J. 170 (2021), 106736.
[42] W.M. Lin, S.X. Lai, D.C. Lu, Q. Zhang, X.L. Lin, J.Q. Lin, J. Wang, Z.F. Huang, An acousto-assisted liquid-marble-based microreactor for quantitative SERS detection of alkaline phosphatase, Sens. Actuators B Chem. 356 (2022), 131361.

**Jingxing Guo** is a postdoctoral researcher in the Department of Medical Imaging, Jinling Hospital, School of Medicine, Nanjing University, China. His research interests span the design and synthesis of facile chemical sensors for on-site analysis in medical diagnosis, food safety and environmental protection.

**Yueqin Liu** is a postdoctoral researcher in the Department of Medical Imaging, Jinling Hospital, School of Medicine, Nanjing University, China. Her researches focus on the study of post-traumatic stress disorder (PTSD)-related neural mechanism.

**Huangxian Ju** received his BS, MS and Ph.D. degrees from Nanjing University during 1982–1992, and was a postdoc in Montreal University (Canada) in 1996–1997. He became an associate and full professor of Nanjing University in 1993 and 1999. He is currently the director of State Key Laboratory of Analytical Chemistry for Life Science. His research interests focus on analytical biochemistry, biosensing and molecular diagnosis. He has authored 81 patents (40 approved), 6 English books, 7 Chinese books and 20 chapters, and published 812 papers in different journals with h-index of 101 (>39,100 citations) and Google Scholar h-index of 111 (> 45000 citations).

**Guangming Lu** is the chair of the Department of Medical Imaging, Jinling Hospital and a Professor in School of Medicine, Nanjing University, China. He received his B.S. degree from Central South University in 1984 and M.S. degree from Peking Union Medical College in 1988. His research interests include the medical imaging and treatment of cardiovascular and cerebrovascular disease, brain disease, and tumors.